IV. CONCLUSIONS

The phenomenon of double bottlenecking, in which a second paramagnetic impurity species participates dynamically in the EPR of a bottlenecked system such as Cu:Mn, has been theoretically predicted and experimentally observed in Cu : Cr, Mn. When suitable parameters prevail, the double-bottlenecking phenomenon enables one to effectively study the EPR of an impurity (in this case Cr) for which EPR cannot be detected by conventional techniques.

[1]P. Monod and S. Schultz, Phys. Rev. **173**, 645 (1968).
[2]J. Owen, M. Browne, W. D. Knight, and C. Kittel, Phys. Rev. **102**, 1501 (1956).
[3]D. L. Cowan, Phys. Rev. Lett. **18**, 770 (1967).
[4]S. Schultz, M. R. Shanabarger, and P. M. Platzmann, Phys. Rev. Lett. **19**, 749 (1967).
[5]A. C. Gossard, A. J. Heeger, and J. H. Wernick, J. Appl. Phys. **38**, 1251 (1967).
[6]H. Hasegawa, Prog. Theor. Phys. **21**, 483 (1959).
[7]L. L. Hirst, Z. Phys. **241**, 9 (1971).
[8]L. L. Hirst, Adv. Phys. (to be published).
[9]L. L. Hirst, Z. Phys. **244**, 230 (1971).
[10]M. D. Daybell and W. A. Steyert, Rev. Mod. Phys. **40**, 380 (1968).
[11]A. Heeger, Solid State Phys. **23**, 248 (1969).
[12]P. Wölfle, W. Brenig, and W. Götze, Z. Phys. **235**, 59 (1970); Phys. Rev. B **2**, 4533 (1970).
[13]Y. Oda and K. Asayama, J. Phys. Soc. Jap. **29**, 869 (1970).
[14]A. C. Gossard, T. Y. Kometani, and J. H. Wernick, J. Appl. Phys. **39**, 849 (1968).
[15]M. D. Daybell and W. A. Steyert, Phys. Rev. Lett. **20**, 195 (1968).
[16]M. Hanabusa and T. Kushida, Phys. Rev. B **5**, 3751 (1972).
[17]D. Davidov, A. Chelkowski, C. Rettori, R. Orbach, and M. B. Maple, Phys. Rev. B (to be published).

PHYSICAL REVIEW B VOLUME 8, NUMBER 1 1 JULY 1973

Determination of Cr-Al Hyperfine and Electric Quadrupole Interaction Parameters in Ruby Using Spin-Echo Electron-Nuclear Double Resonance*

P. F. Liao and S. R. Hartmann
Columbia Radiation Laboratory, Department of Physics, Columbia University, New York, New York 10027
(Received 31 January 1973)

Electron-spin-echo–electron-nuclear-double-resonance (ENDOR) spectra have been observed in dilute ruby crystal at magnetic fields of 1.7, 3.3, 5.8, and 7.5 kG. Analysis of the data yields the Cr-Al hyperfine and electric quadrupole interaction parameters for 34 Al nuclear neighbors, and shows the Al nuclear quadrupole Hamiltonian must include an asymmetry parameter and a tilt of the principal axis of the electric field gradient away from the direction of the crystal optic axis. The parameters are used to calculate electron-spin-echo behavior, and the comparison with experimentally determined spin-echo modulation data is excellent. Explicit expressions for the double-resonance effect are derived under limiting conditions and show the sinusoidal dependence of the double-resonance amplitude on the time separation of the first two excitation pulses. Various properties of the echo-ENDOR effect and its capability to untangle overlapping resonances are experimentally demonstrated.

I. INTRODUCTION

Ruby (Cr^{3+}-doped Al_2O_3) is a crystal of great general interest. It is a material of technological importance both as a solid-state maser[1] and as a laser,[2] and consequently there have been extensive investigations of its electronic[3] and optical[4] properties. The technology and interest associated with ruby were undoubtedly major factors in its being chosen as the material in which to perform the first photon-echo[5] and self-induced-transparency[6] experiments.

Conventional electron-spin-resonance,[3] acoustic-paramagnetic resonance,[7] electron-nuclear-double-resonance (ENDOR),[8] and electron-spin-echo[9] experiments have been used to study the $^2A_4$ electronic ground state of Cr^{3+} in ruby. A study[10] of the linewidth of EPR transitions in the $^2A_4$ ground state as a function of chromium concentration has shown a concentration-independent contribution which is almost entirely due[11] to the unresolved superhyperfine interactions between the Cr^{3+} ion and the magnetic moments of neighboring aluminum nuclei. Using conventional ENDOR[12] techniques, Laurance, McIrvine, and Lambe[8] made the first measurements of the nuclear-magnetic-resonance spectra of the nearest 13 aluminum neighbors to the Cr^{3+} ion, and obtained values for parameters describing the Cr-Al interaction and the Al electric quadrupole interaction. Using these parameters, it is possible to understand the electron-spin-echo behavior for short excitation-pulse separations.[9,13]

Later experiments[14] with longer pulse separations were, however, not in good agreement with a theory which used the ENDOR results of Ref. 8. This discrepancy between experiment and theory lead us to repeat the ENDOR experiment using the pulsed technique of echo ENDOR.[15] This method, which was first used by Mims,[16] is the extension to an electron-spin system of a double-resonance technique used in nuclear magnetic resonance.[17] We find that the echo-ENDOR technique is very well suited for the determination of the Cr-Al hyperfine interaction parameters in ruby, especially since it allows one to disentangle the overlapping resonances associated with the many neighboring Al nuclei and leads to an unambiguous assignment for closely lying lines. Our results show that the interaction Hamiltonian for ruby must (i) include an asymmetry parameter to allow for a noncylindrically symmetric electric field gradient and (ii) allow the principal axis of the field gradient to point in a direction away from the optic axis. The interaction parameters we obtain describe the ENDOR spectra of 34 neighboring nuclei over a wide range of applied magnetic fields and greatly improve agreement between theory and experiment for electron-spin-echo behavior for short *and* long excitation-pulse separation times.

The echo-ENDOR technique consists of monitoring the amplitude of the three-pulse stimulated echo[18] as a function of the frequency of a double-resonance rf field applied to the sample in the time interval between the second and third excitation pulses (Fig. 1). Nuclear double resonance is indicated by a decrease in echo amplitude. In Sec. II, we reanalyze the echo-ENDOR method using the density matrix to obtain, under limiting conditions, explicit expressions for the double-resonance signal amplitude of a system such as ruby (Al_2O_3: Cr^{3+}) whose Al nuclei have $I=\frac{5}{2}$. Our result reduces to Mim's result[16] for $I=\frac{1}{2}$ and shows the sinusoidal dependence of double-resonance amplitude on τ_1(the time separation of the first two excitation pulses) which we exploit to analyze the complicated ruby ENDOR spectra. In the Appendix, we present a simple vector model of the echo-ENDOR effect.

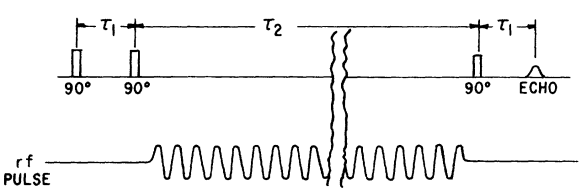

FIG. 1. Spin-echo–ENDOR pulse sequence.

The apparatus is described in Sec. III. In Sec. IV we test experimentally the behavior of the double-resonance amplitude as a function of τ_1, the nuclear species resonated, and the amplitude of the double-resonance rf magnetic field. The technique used for untangling overlapping resonances is also demonstrated. The echo-ENDOR spectra of ruby and its analysis is presented in Sec. V. The results given here represent a refinement of preliminary measurements which were reported earlier.[18] In this latter section, we make a comparison between experimentally obtained[14] spin-echo modulation behavior and the corresponding behavior obtained from a theoretical calculation which uses the interaction parameters obtained from the echo-ENDOR experiment. Comparison is made with *X*-band and *Ku*-band data, and agreement is excellent.

II. THEORY

Mims[16] has given an expression for the echo-ENDOR effect for the case in which a nuclear neighbor has spin-$\frac{1}{2}$. For completeness and to facilitate a direct comparison with our echo-ENDOR results in ruby, we reanalyze the effect using a density-matrix formulism which is valid for arbitrary nuclear spin. Our result reproduces that of Mims and in addition gives the effect of equivalent neighbors and the dependence on the amplitude of the double-resonance rf field.

We describe the echo atom as a two-level system[13] and hence, in the absence of the radiation field, the Hamiltonian for the echo atom and its nuclear neighbors can be written in terms of the Pauli spin matrices:

$$\mathcal{H}=\tfrac{1}{2}(H_1+H_2)\sigma_0+\tfrac{1}{2}(H_1-H_2+\hbar\omega)\sigma_3\,, \tag{1}$$

where H_1 and H_2 are the nuclear Hamiltonians corresponding to the echo atom being in state 1 and 2, respectively, and the energy separation between the echo states is $\hbar\omega$. Because we have assumed the energy corresponding to ω is much greater than nuclear energies, we have dropped off-diagonal terms and kept only terms proportional to σ_0 and σ_3.

The echo amplitude is given by the expectation value of the dipole moment,

$$\langle\vec{P}\rangle=\mathrm{Tr}\,\vec{P}\rho,\quad \langle P\rangle=\hbar\gamma(S_x\hat{x}+s_y\hat{y}),$$
$$S_x=\tfrac{1}{2}\sigma_1,\quad S_y=\tfrac{1}{2}\sigma_2. \tag{2}$$

For the case of the familiar two-pulse echo the density matrix ρ is given by

$$\rho(\tau+\tau_1)=e^{-i\mathcal{H}\tau/\hbar}R_{180}e^{-i\mathcal{H}\tau_1/\hbar}R_{90}\rho_0 R_{90}$$
$$\times e^{i\mathcal{H}\tau_1/\hbar}R_{180}e^{i\mathcal{H}\tau_1/\hbar}\,, \tag{3}$$

where R_{90} and R_{180} are operators giving the effects of the 90° and 180° excitation pulses, respectively. The term τ measures the time after the 180° pulse, and ρ_0 is the initial density matrix. For the stimulated-echo case and echo ENDOR, R_{180} is replaced by $R_{90}UR_{90}$,

$$R_{180} \rightarrow R_{90}UR_{90} . \tag{4}$$

The operator U gives the time development between the second and third 90° pulse of the stimulated-echo-pulse sequence and also contains the effect of the rf field on the nuclear neighbors.

To calculate the stimulated-echo amplitude we shall make some simplifying assumptions concerning the action of the time-development operator U.

First, we shall assume that the time between the second and third pulses is sufficiently long that all phase memory of the system is irreversibly lost. This statement amounts to setting all off-diagonal matrix elements of the density matrix to zero, with the density matrix written in a representation in which the Hamiltonian is diagonal.

Next, we shall assume that the effect of the rf field, which is applied during almost the entire time between the second and third microwave pulses, can be replaced by an operator which acts only immediately preceding the third pulse. We assume the rf field couples together only two energy states of a nucleus in the field of a given echo-atom state. If we were to assume the rf pulse to be a 180° pulse, the effect of this operator would be to interchange the matrix elements of the density matrix corresponding to the two nuclear energy states involved in the transition. In the more general problem of an arbitrary θ-degree pulse, we treat the two energy states involved as a two-level system and apply the 2×2 rotation operator corresponding to a θ-degree rotation. With these assumptions and further assuming δ-function excitations, we find that the trace over the electron-spin states is easily taken to yield the stimulated-echo amplitude

$$\langle P\rangle_{\text{ste}} = \left(\frac{C}{4}\right)\sum_{l=1}^{2} \mathrm{Tr}(e^{(iH_1\tau/\hbar)}\, e^{-iH_2\tau/\hbar}\, U_l \times e^{-iH_1\tau_1/\hbar}\, e^{iH_2\tau_1/\hbar}\, U_l^{-1}\, e^{i\omega(\tau-\tau_1)} + \text{H. c.}), \tag{5}$$

where $U_{1,2}$ are defined such that

$$U = \tfrac{1}{2}(U_1+U_2)\sigma_0 + \tfrac{1}{2}(U_1-U_2)\sigma_3, \tag{6}$$

and H. c. denotes the Hermitian conjugate of the operators to its left. Note that the term U_1 (U_2) will contain the effect of the rf field only if the nuclear transition corresponds to the nucleus being in the field of the echo atom in state 1 (state 2). Additional terms which are proportional to $e^{\pm i\omega(\tau_1+\tau)}$ have been dropped, as these will not contribute to the echo after an average is taken over the line shape. The number C is a normalization constant dependent on the temperature. The nuclei have been treated in the high-temperature limit.

It is interesting to compare this expression with that obtained for the two-pulse echo:

$$\langle P\rangle_{\text{2PE}} = C\,\mathrm{Tr}(e^{iH_1\tau/\hbar}\, e^{-iH_2\tau/\hbar}\, e^{-iH_1\tau_1/\hbar} \times e^{iH_2\tau_1/\hbar}\, e^{i\omega(\tau-\tau_1)} + \text{H. c.}) . \tag{7}$$

If $[H_1, H_2] = 0$, we can write

$$\langle P\rangle_{\text{2PE}} = C\,\mathrm{Tr}\{\exp[(i/\hbar)(H_1 - H_2 + \hbar\omega)(\tau-\tau_1)] + \text{H. c.}\} . \tag{8}$$

The form of this expression is very suggestive. Note that $(1/\hbar)\langle H_1 - H_2 + \hbar\omega\rangle\,\tau_1$ is just the phase gained by the dipoles during the time τ_1, and for $\tau = \tau_1$ it is exactly cancelled in the formation of the echo. Such would also be the case with stimulated echoes except for the operator U which, if it induces a nuclear transition, can cause an incomplete cancellation of the phase and hence a degradation of the echo. For this special case of $[H_1, H_2] = 0$, the expression for the stimulated echo is easily evaluated. We can then decompose H_1, H_2, and U and write

$$H_{1,2} = \sum_j h_{1,2}^j, \qquad U = \prod_j U^j, \tag{9}$$

where the superscript j refers to the jth nuclear neighbor. Note that for those nuclei which are not resonant with the rf field, $U_{1,2}^j$ is simply the identity matrix. Let the rf field be resonant with nuclei which we will label k, and let the frequency be such that transitions are induced from the lth to the mth energy states of these nuclei corresponding to the echo atom in state 1 or 2. (With our approximations the equations are symmetric with respect to these states.) Evaluating the nuclear traces at the time of the echo we obtain

$$\langle P\rangle_{\text{ste}} = \frac{C}{4}\left(1 + \prod_k \frac{1}{2I_k+1}\{2I_k - 1 + 2\cos^2\tfrac{1}{2}\theta + 2\sin^2\tfrac{1}{2}\theta\cos[(\omega_{lm}^{1k} - \omega_{lm}^{2k})\tau_1]\}\right)\hat{x}, \tag{10}$$

where

$$\omega_{lm}^{1k} = (1/\hbar)(E_{1_l}^k - E_{1_m}^k), \quad \omega_{lm}^{2k} = (1/\hbar)(E_{2_l}^k - E_{2_m}^k);$$

$E_{1\alpha}^k$ and $E_{2\alpha}^k$ are the energy eigenvalues of h_1^k and h_2^k, respectively.

In our experiments at high fields, the nuclear Hamiltonians are nearly diagonal, and the above expression should quite accurately describe our observations.

III. EXPERIMENTAL APPARATUS

Experiments were performed at two microwave frequencies, 16.2 and 9.3 GHz, corresponding to *Ku* and *X* bands, respectively. Because of the

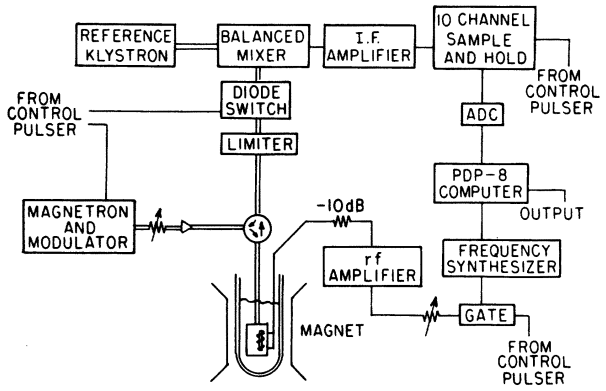

FIG. 2. Spin-echo–ENDOR spectrometer.

large difference in these frequencies, two separate microwave spectrometers were used. The two spectrometers are essentially identical in design and utilize a superheterodyne scheme for the detection of echoes. The essential components of the spin-echo–ENDOR spectrometer are shown schematically in Fig. 2. The sample is enclosed in a coil and mounted in a rectangular low-Q cavity, which is immersed in liquid helium. Most of the experiments were performed with the liquid helium pumped below the λ point to prevent bubbling. This procedure eliminates a major source of noise. At X band the cavity operates in the TE_{101} mode; and in the TE_{103} mode at Ku-band frequencies. All experiments used a 0.005-wt%-Cr ruby sample whose dimensions were 1 cm in diameter and 1 mm thick.

Some care must be taken in winding the coil around the sample and placing the sample and coil into the cavity. By mounting the coil and sample as shown in Fig. 3, the sample will be located in a region of maximum microwave magnetic field assuring a high filling factor. Furthermore, with the coil placed in the orientation shown, its effect on the microwave properties of the cavity is minimized, and microwave fields are allowed to penetrate into the sample. The coil is such that the microwave electric fields are essentially perpendicular to the coil windings, while the microwave magnetic fields lie in the plane of the coil turns. Hence, little current is induced in the coil by the microwave fields.

The microwave pulses required to produce the stimulated echo are generated by a 500-W pulsed magnetron. These 30-nsec pulses are guided to the microwave cavity by a circulator. A Gordon variable coupler[19] assures excellent coupling between waveguide and cavity. When the spins in the sample rephase to form the echo pulse, the circulator directs this pulse to the balanced mixer. A combination of a limiter and diode switch is used to protect the receiver circuitry from being saturated by the high-power magnetron pulses. After the final magnetron pulse, the diode switch is turned on so that the echo signal reaches the mixer unattenuated. The echo-pulse signal is beat with the local oscillator output, whose frequency has been tuned 30 MHz above or below that of the magnetron. The resulting 30-MHz pulse produced by the mixer is amplified and then detected and measured with an analog-to-digital converter (ADC) whose output is stored in a PDP-8 computer for averaging purposes. Actually because the echo-pulse width is too short to be accurately measured by the ADC, it is first sent to a ten-channel sample and hold. This instrument covers a 1-μsec interval with each of the ten consecutive channels having an amplitude proportional to the average pulse height during a 100-nsec period. These ten channels are then digitized by the ADC with a digitizing time of 25 μsec per channel and stored in the computer. The rf field necessary to induce nuclear transitions is generated as follows: The output of a frequency synthesizer is gated to produce an rf pulse. This pulse is timed to occur between the second and third microwave excitation pulses. Typically, the time separation between these pulses is 120 μsec and the length of the rf pulse is 100 μsec. The pulse is amplified and sent through an attenuator (10 dB) to the coil which is wrapped around the sample. Use of the attenuator effectively decouples the coil from the rf amplifier circuitry, and no impedance matching is required. Furthermore, as the 3-W amplifier has a very broad bandwidth, no tuning of the rf apparatus is needed during the experiment.

Data taking is completely automated. The PDP-8 computer is interfaced into the frequency synthesizer and thus it both controls the frequency output of the synthesizer as well as measures the stimulated-echo amplitude. The computer is typically programed to sweep the rf frequency over a 1-MHz range in 2-kHz steps while storing the echo amplitude as a function of rf frequency. Usually nine such sweeps are averaged together, which gives a factor of 3 increase in the signal-to-noise ratio, before the computer plots the spectra by means of a digital-to-analog converter and an X-Y

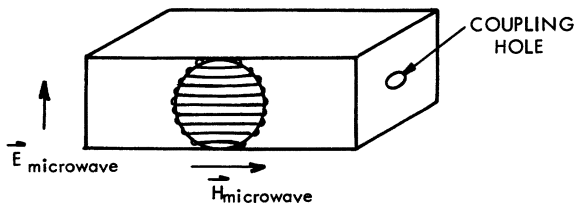

FIG. 3. Placement of sample and coil in cavity.

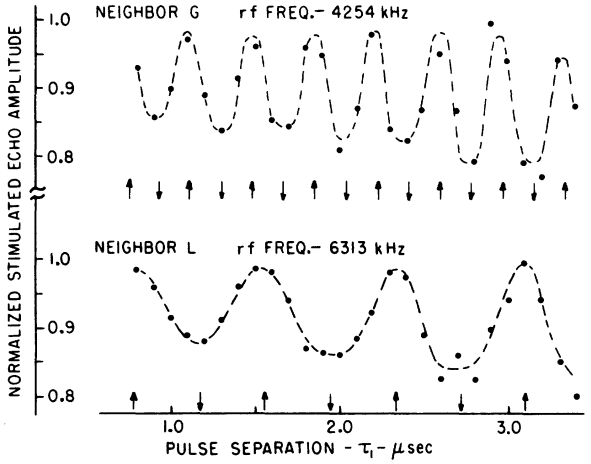

FIG. 4. Normalized stimulated echo amplitude vs pulse separation τ_1 at 7.5 kG. Upper curve with rf pulse tuned to a neighbor set G transition. Lower curve with pulse tuned to neighbor set L transition.

recorder. Data are also punched out on paper tape, so they are preserved in digital as well as analog form. The computer is easily programed to manipulate the data, and particular portions of the spectra can be examined in detail if required. Because of the long spin-lattice relaxation time of ruby at liquid-helium temperatures, the rate at which data can be accumulated is limited to about 3 pulse sequences per second.

IV. PROPERTIES OF SPIN-ECHO-ENDOR IN RUBY

The experimental spin-echo–ENDOR spectra have a number of characteristics that can be obtained directly from Eq. (10). First, we notice that the ENDOR effect has a sinusoidal dependence on the time separation τ_1 between the first and second microwave pulses. The period of this sinusoid is determined by the difference in the nuclear frequencies corresponding to the echo atom in state 1 or in state 2. This difference is, in turn, determined by the strength of the hyperfine interaction of the nuclear neighbor with the Cr^{3+} ion. The sinusoidal dependence on τ_1 is shown in Fig. 4, where we have plotted the ratio of the experimental stimulated echo amplitude obtained with the rf double-resonance pulse applied to the amplitude obtained with no rf double-resonance pulse applied. The frequency of the rf field is set to exact resonance with a nuclear transition. We plot the ratio rather than simply the echo amplitude to eliminate the effect of dephasing interactions which cause the echo to decay and to remove any echo envelope modulation effects that are present. This procedure serves as a kind of normalization. The upper curve in Fig. 4 shows the ratio when the rf is set to a frequency corresponding to a transition of nuclear neighbor G (see Ref. 8 for notation), while the lower curve gives data for a transition associated with nuclear neighbor set L. The curve drawn through the data points is to serve as a visual aid in following the data. The strength of the hyperfine interaction of neighbor G is approximately twice that of neighbor L, and the periods of oscillation shown in Fig. 4 reflect this fact. We also show in Fig. 4 the positions of stimulated echo maxima and minima as predicted by Eq. (10). Pulse separations that give echo maxima are indicated with an upward pointing arrow, while the predicted minima have a downward pointing arrow. The agreement with Eq. (10) is very good even after many cycles of the oscillation.

Because of this dependence of the echo-ENDOR effect on the pulse separation τ_1, echo ENDOR has an important advantage over standard ENDOR[8,12] techniques. One can use the dependence of a particular line on pulse separation as a kind of signature which helps in the identification of the line and in associating it with a particular neighbor site. The lines are grouped in pairs as a given nuclear transition has the same dependence on τ_1 when in the field of an echo atom which is in either state 1 or state 2. If the nuclei involved have spin I, greater than $\frac{1}{2}$, and have a quadrupole moment, as is the case with aluminum in ruby, then each nucleus will give rise to a set of $2I$ resonance lines due to the unequal energy separations of the nuclear states. This multiplicity of lines can be confusing; however, an additional simplification occurs in our case where the electric quadrupole Hamiltonian is independent of the echo-atom state. In this case the difference in the nuclear frequencies corresponding to the echo atom in state 1 or state 2 will be the same for all allowed nuclear transitions. Hence, as indicated by Eq. (10), all of the echo-ENDOR lines belonging to a particular nuclear neighbor set have the same dependence on pulse separation. We are able to use this signature to further classify the lines together.

In addition, if lines corresponding to different neighbor sets happen to overlap, one can separate the lines by choosing the pulse separation τ_1 correctly. Figure 5 shows echo-ENDOR spectra in regions in which there are transitions ($m = \frac{3}{2} \leftrightarrow \frac{1}{2}$) and ($m = -\frac{1}{2} \leftrightarrow -\frac{3}{2}$) of nuclear neighbor set I at 6.80 and 7.36 MHz, respectively. The upper curves were taken with $\tau_1 = 1.0$ μsec. The ($m = -\frac{1}{2} \leftrightarrow -\frac{3}{2}$) I transition overlaps transitions due to neighbors V and S in the region 7.36 MHz. By monitoring the I line at 6.80 MHz, we adjusted the pulse separation to 3.3 μsec, for which I transitions produce no double-resonance signals. The V and S lines at 7.36 MHz were then clearly re-

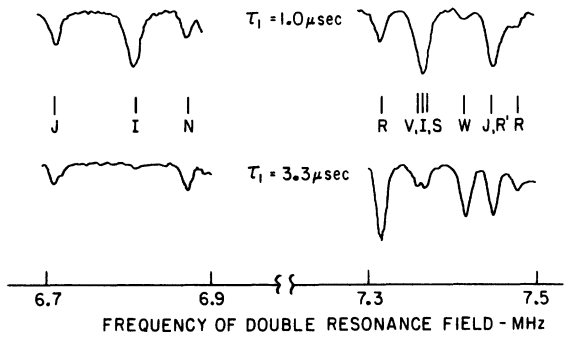

FIG. 5. Echo-ENDOR spectra at 7.474 kG with $\tau_1 = 1.0$ and 3.3 μsec.

solved as shown on the lower curve of Fig. 5.

In principle, the sinusoidal dependence of the echo-ENDOR effect allows one to determine the hyperfine interaction constants by a kind of Fourier-transform spectroscopy. One would measure the intensity of the echo-ENDOR lines as a function of pulse separation and then obtain the Fourier-transform of such data. A technique such as this might be particularly useful if a great number of lines are excited by the rf pulse at once; however, it requires that the homogeneous lifetime T_2 of the echo atom be long enough to permit measurement of echoes over a range of pulse separations sufficient enough to obtain the desired resolution. In the present case of ruby, this technique was not attempted because T_2 is approximately 1.0 μsec for the sample concentration used (0.005-wt% Cr), and much greater resolution could be obtained by direct measurement of the spectra.

As might have been intuitively expected, Eq. (10) indicates that the echo-ENDOR effect disappears for a 360° rf pulse. In this case, the nucleus returns to its initial state, and there is no change in the local field at the echo-atom site. Figure 6 shows this effect. The ENDOR line disappears only at exact resonance because the effective field in the rotating frame of the nucleus has an additional component in the direction of the local field when the rf frequency is not equal to the resonance frequency. In fact, the echo-ENDOR effect does not disappear completely even at exact resonance because of inhomogeneities in the rf field. The dependence of the double-resonance signal on rf amplitude is also often helpful in the identification of ENDOR lines. The angle θ, which describes the interaction of the nucleus with the rf pulse, is given by the following expression:

$$\theta = \gamma h_{rf} \tau_{rf} \langle m \mid I_x \mid m+1 \rangle$$

$$= \gamma h_{rf} \tau_{rf} [I(I+1) - m(m+1)]^{1/2}, \qquad (11)$$

where h_{rf} is the component of the rf field perpendicular to the local field at the nuclear site, τ_{rf} is the length of the rf pulse, and γ is the gyromagnetic ratio of the nuclei. If more than one nuclear species is present this expression and Eq. (10) help one to determine, from the relative behavior of different ENDOR lines, which species and m state is responsible for the line in question.

The echo-ENDOR technique has very good sensitivity. No matter how small the interaction between the nucleus and the echo atom may be, one can always obtain a large signal by correctly adjusting the pulse separation τ_1. All that is required is to be able to detect and measure the stimulated echo. Note that those nuclei which are resonant with the rf pulse do not simply prevent an echo atom from contributing to the echo but may actually produce an echo that is 180° out of phase with the normal echo. This considerably enhances the double-resonance signal.

Because ENDOR spectra have been measured in ruby with conventional techniques,[8] it is possible to make a direct comparison with echo ENDOR. Our echo-ENDOR spectra show a great number of nuclear resonances which were not observed before, indicating their high sensitivity. The resolution of each method appears to be about the same. In the echo-ENDOR experiment, the resolution is determined, in part, by the duration

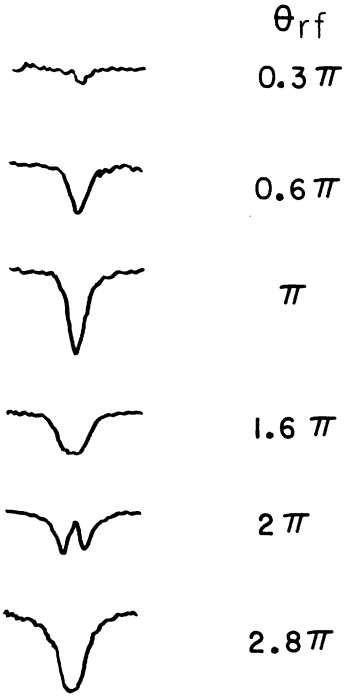

FIG. 6. Echo-ENDOR vs rf-field amplitude. Spectra between 4.2 and 4.3 MHz at 7.5 kG, $\tau_1 = 1.3$ μsec, $\tau_2 = 120$ μsec.

of the rf pulse through Heisenberg's uncertainty principle. We were able to use long pulse separations that allowed sufficiently long rf pulses such that the uncertainty principle did not broaden the line shapes. The generation of echoes does not require the careful balancing of a microwave bridge that is necessary in all high-sensitivity cw spectrometers; and, since it is a pulsed experiment, it is relatively free of microphonics which would be a problem in the conventional ENDOR technique. The echo-ENDOR effect should not depend on any balance of relaxation rates as the conventional ENDOR effect may,[20] and hence one can always be relatively confident of observing double-resonance signals whenever one can observe echoes.

It should be noted that for the aluminum resonances ($I=\frac{5}{2}$) in ruby, Eq. (10) predicts a decrease in echo amplitude of nearly 50% for three equivalent nuclei. However, experimentally the decrease was often much less, frequently only 10%. While the exact mechanism responsible for the small signals is not understood, they may result from interactions that broaden the nuclear resonance lines. The rf pulse is then unable to excite the entire nuclear line resulting in a smaller ENDOR signal. Some of the resonance lines seem unusually broad. Lines associated with the $-\frac{1}{2}$ electron-spin state in a magnetic field of 1.7 kG were very broad and at 3.3 kG those associated with the $+\frac{1}{2}$ state were apparently so broad that no double-resonance signal could be detected for them at all.

Because electron-spin echoes in ruby can only be observed when the magnetic field is applied nearly parallel to the crystal's optic axis,[9,13] the measurement of echo-ENDOR spectra is restricted to this orientation of the magnetic field. All our measurements were made with the field aligned along the optic axis to an estimated precision of 0.25°. Conventional ENDOR techniques are also restricted to this orientation of the magnetic field as no ENDOR signals have been seen at other angles.[8]

V. ALUMINUM HYPERFINE AND ELECTRIC QUADRUPOLE INTERACTION PARAMETERS IN RUBY

The nuclear-magnetic-resonance spectrum of aluminum nuclei in the immediate neighborhood of the Cr^{3+} ion was first observed and analyzed by Laurance, McIrvine, and Lambe[8] using conventional ENDOR techniques. Their paper gives an excellent discussion of the physical mechanisms responsible for the interaction between the aluminum nuclei and the Cr^{3+} ion.

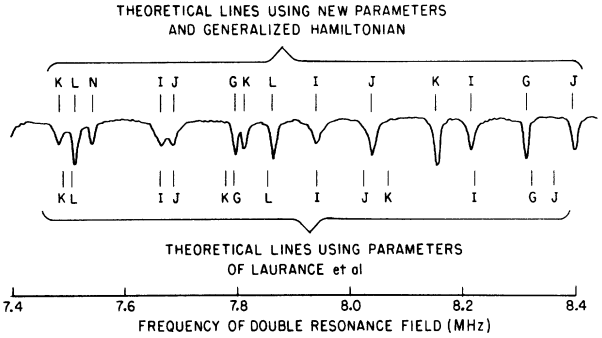

FIG. 7. Spin-echo–ENDOR spectra at 5.815 kG in region 7.4–8.4 MHz.

Our initial echo-ENDOR experiments[15] indicated a small but significant discrepancy with the analysis of Laurance, McIrvine, and Lambe. Subsequent experimental results, which we report here, confirm these experiments and allow the determination of additional interaction parameters. Figure 7 shows a small portion of our data. In it we plot the stimulated-echo amplitude versus frequency of the double-resonance field. The dips result from aluminum nuclear resonances and are associated with the nearest 13 aluminum neighbors labeled G, I, J, K, L (notation of Ref. 8) and the 14th nearest neighbor N. The lines drawn below the data give the resonance positions calculated with the Hamiltonian and interaction parameters given by Laurance *et al.* While there is good agreement for neighbors G, I, and L, there is considerable error for neighbor sets J and K. This discrepancy can be removed by the use of a more general Hamiltonian.

The ruby lattice Al_2O_3, has threefold symmetry about the crystal's optic axis; hence, it is natural to expect the crystalline electric field gradient to possess the same symmetry. The replacement of an aluminum atom with a Cr^{3+} ion, however, breaks the symmetry for the neighboring aluminum nuclei. In fact, the presence of the Cr^{3+} ion actually induces as much as a 44% change in the magnitude of the electric field gradient. It is therefore not unreasonable to expect the electric field graient to take an arbitrary form, and the spin Hamiltonian must reflect this fact.

A Hamiltonian which includes an electric quadrupole interaction Hamiltonian of arbitrary symmetry can be written as follows:

$$\mathcal{H}=g\mu_B HS_z+D[S_z^2-\tfrac{1}{3}S(S+1)]+\sum_j\{-\hbar\gamma HI_z^j+S_z[(A+B_z)^jI_z^j+B_t^jI_1^j]$$
$$+Q^j e^{-i\theta_1 I_2^j}e^{-i\theta_2 I_1^j}e^{-i\theta_3 I_z}[I_z^{j2}+\tfrac{1}{3}\eta(I_1^{j2}-I_2^{j2})]e^{i\theta_3 I_z^j}e^{i\theta_2 I_1^j}e^{i\theta_1 I_2^j}\}. \quad (12)$$

The subscripts 1, 2 refer to directions in the transverse plane parallel to and perpendicular to the transverse component of the local field at the aluminum neighbor site, respectively. This Hamiltonian differs from that of Laurance *et al.* by the introduction of the asymmetry parameter η, and a tilt of the principal axis of the electric field gradient determined by θ_1, θ_2, and θ_3. From perturbation theory we obtain the ENDOR frequencies

$$\Delta E(m \rightarrow m+1) = \omega_c - P''' + (m+\tfrac{1}{2})P' + (m+\tfrac{1}{2})^2 P'', \tag{13}$$

where

$$P' = Q\{3\cos^2\theta_2\cos^2\phi - 1 + \eta[\cos 2\theta_3(\sin^2\phi - \cos^2\phi\sin^2\theta_2) - \sin 2\theta_3 \sin\theta_2 \sin 2\phi]\},$$

$$P'' = (Q^2/3\omega_c)[36(\phi^2+\theta_2^2) - \eta^2],$$

$$P''' = (8Q/9\omega_c)[18(\phi^2+\theta_2^2) - \eta^2],$$

$$\omega_c = (\gamma/2\pi)\,|H_{eff}|, \quad \varphi = \theta_1 - \theta,$$

$$\tan\theta = B_t S_z/[(A+B_z)S_z - (\gamma/2\pi)H],$$

$$\vec{H}_{eff} = \{[(A+B_z)S_z - (\gamma/2\pi)H]\hat{z} + B_t S_z \hat{e}_1\}(2\pi/\gamma),$$

and where P'' and P''' are of second order in η, θ_1, and θ_2.

The interaction constants of the nearest 14 neighbors given in Table I were determined by a least-squares fit to our spin-echo–ENDOR data using Eq. (13). The least-squares-fitting program was performed on a PDP-8 minicomputer which enabled us to interact directly with the fitting procedure. As is often the case, when fitting nonlinear functions of many variables, frequent restarts of the program were necessary, and the "on-line" capability of a small computer permitted a fairly rapid fit. The minimization algorithm of Fletcher and Powell[21] was used in the program.

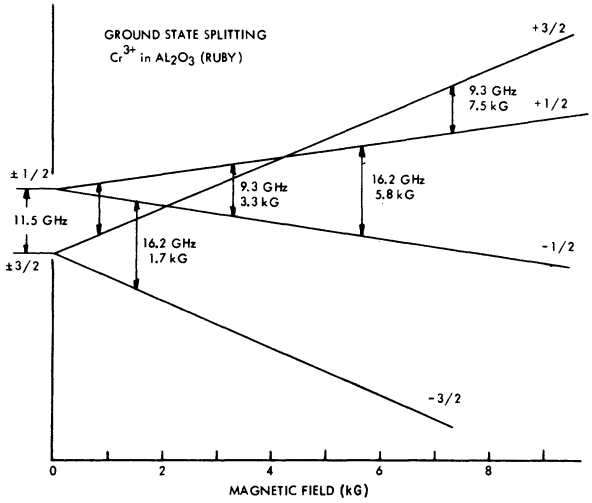

FIG. 8. Energy-level diagram of splitting for Cr^{3+} ion in Al_2O_3 vs magnetic field. The magnetic field is applied parallel to the crystalline optic axis. Labeled transitions correspond to transitions at which echo ENDOR was performed.

Our data were measured at four magnetic fields corresponding to the microwave transitions at 9.3 and 16.2 GHz for which spin echoes could be observed. These transitions are indicated on the

TABLE I. Cr-Al interaction constants in ruby.

Neighbor set	*G*	*I*	*J*	*K*	*L*	*N*
$A+B_z \pm 0.002$ MHz	2.694	2.422	2.453	2.065	1.398	0.701
$B_t \pm 0.03$ MHz	0.0	0.444	0.945	0.844	0.822	0.0
$2Q \pm 0.01$ MHz	0.520	0.281	0.382	0.398	0.354	0.371
$\theta_1 \pm 0.03$ rad	0.0	−0.075	−0.130	−0.284	−0.028	0.0
$\theta_2 \pm 0.1$ rad	0.0	0.0	0.144	0.055	0.0	0.0
$\theta_3 \pm 0.5$ rad	0.0	0.0	0.0	0.0	0.0	0.0
$\eta \pm 0.5$	0.0	0.0	−0.1	−0.425 ± 0.1	0.0	0.0
Coordinates of neighbors as assigned in Ref. (8) in terms of rhombohedral cell dimension $a_0 = 5.137$ Å with Cr^{3+} ion at origin	0.0	0.27	−0.27	−0.27	0.27	0.0
	0.0	0.46	−0.46	−0.46	0.46	0.0
	−0.53	−0.11	−0.42	0.31	0.42	0.73
		0.27	−0.27	−0.27	0.27	
		−0.46	0.46	0.46	−0.46	
		−0.11	−0.42	0.31	0.42	
		−0.54	0.54	0.54	−0.54	
		0.0	0.0	0.0	0.0	
		−0.11	−0.42	0.31	0.42	

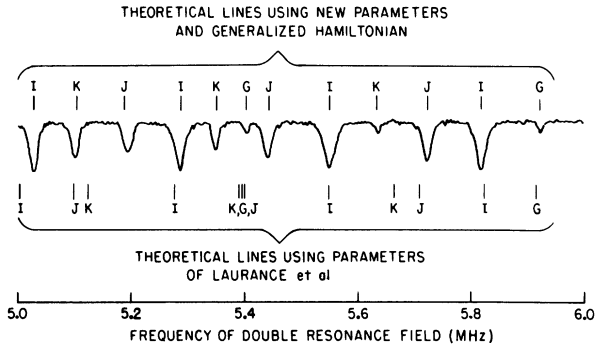

FIG. 9. Spin-echo–ENDOR spectra at 1.696 kG in region 5.0–6.0 MHz.

energy-level diagram shown in Fig. 8. The 9.3-GHz transition at 800 G was not used because echoes could not be observed at that field. The data included all the electron-spin states involved in the microwave transitions with the exception of $S_z = \frac{1}{2}$ at 3.3 kG and $S_z = -\frac{1}{2}$ at 1.7 kG. As mentioned in Sec. II, no ENDOR lines were observed for $S_z = +\frac{1}{2}$ at 3.3 kG, and the lines were too wide to be resolved for $S_z = -\frac{1}{2}$ at 1.7 kG.

Our preliminary experiments[18] contained insufficient data to determine θ_2, θ_3, and η. The results given here are in agreement with the previous experiment and in addition show a nonzero asymmetry parameter and θ_2 for nuclear neighbor sets K and J. The lines drawn above the data in Fig. 7 indicate resonance positions calculated by diagonalizing the generalized nuclear Hamiltonian with an IBM-360 computer and using the interaction parameters for the nearest 14 neighbors given in Table I. The agreement between theory and experiment shown in Fig. 7 is typical for all of the data. Figure 9 shows some additional spectra which were taken at 1.696 kG. The spectra in Fig. 7 were taken at 5.815 kG. At the lower field the discrepancy with the results of Laurance *et al.* is slightly more pronounced, but the generalized Hamiltonian continues to give a good fit. The reason for the very small remaining disagreement is not clear at the present time. It may be due to a slight error introduced by perturbation theory at low fields or from interactions which were not included in the Hamiltonian. Such interactions include the dipole-dipole interaction between aluminum nuclei.[22]

As can be seen in Table I, there is a significant tilt of the electric field gradient's principal axis for nuclear sets J and K. Neighbor set K also has a large asymmetry parameter. The value of $2Q$ for an aluminum nucleus, which is unaffected by the Cr impurity, is 0.36 MHz.[23] For sets J and K we find the strain-induced change in $2Q$ (from 0.36 MHz) of +0.022 and +0.038 MHz, respectively, which is opposite in sign to the values of −0.02 and −0.07 previously reported.[8]

In addition to resonances due to the nearest 13 neighbors, echo-ENDOR lines associated with much further nuclei were observed. These lines had not been detected before. Because the further nuclei are not bonded to any oxygen atom in common with the Cr^{3+} ion, the transferred hyperfine interaction (which is represented by the interaction constant A) is expected to be small. In Table II we give the values of the interaction constants for those further neighbors which could be

TABLE II. Cr-Al interaction constants in ruby for further neighbors.

Neighbor set	P	P'	R	R'	S	W	V
$A + B_z$(± 0.01 MHz)	−0.206	−0.190	−0.169	0.180	0.148	0.103	0.152
B_t(± 0.1 MHz)	0.0	0.0	0.20	0.10	0.15	0.08	0.0
$2Q$(± 0.02 MHz)	0.361	0.365	0.364	0.376	0.351	0.360	0.351
(B_z) point dipole	−0.188	−0.188	0.172	0.172	0.147	0.107	0.148
(B_t) point dipole	0.0	0.0	0.20	0.20	0.15	0.08	0.0
Coordinates of	0.0	0.0	0.27	0.27	0.54	−0.54	0.0
nuclear neighbors[a]	0.93	−0.93	0.46	0.46	0.0	0.0	0.0
	0.0	0.0	0.84	0.84	0.95	0.16	1.27
	0.80	−0.80	0.27	0.27	−0.27	0.27	0.0
	−0.46	0.46	−0.46	0.46	0.46	−0.46	0.0
	0.0	0.0	−0.84	0.84	0.95	1.15	−1.27
	−0.80	0.80	−0.54	0.54	−0.27	0.27	
	−0.46	0.46	0.0	0.0	−0.46	0.46	
	0.0	0.0	−0.84	0.84	0.95	1.15	

[a]Coordinates given in terms of rhombohedral cell dimension $a_0 = 5.137$ Å. The assignments of data to set P or P' (R or R') is arbitrary.

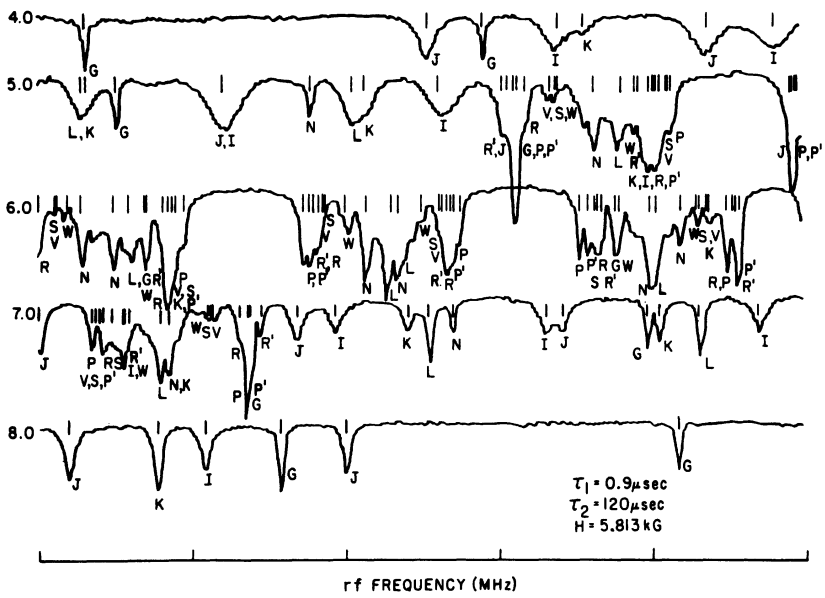

FIG. 10. Complete spin-echo–ENDOR spectra at 5.813 kG.

positively identified. Also tabulated are the values of B_z and B_t calculated with a point-dipole interaction. In all cases the point-dipole interaction is in relatively good agreement with the observed values of $A+B_z$ and B_t.

In Fig. 10, we show the complete double-resonance spectrum which is observed at 5.8 kG for fixed excitation pulse separations of $\tau_1 = 0.9$ μsec and $\tau_2 = 170$ μsec. The spectrum covers the frequency range 4.0–9.0 MHz and appears exceedingly complex. However, by carefully exploiting the characteristics of the echo-ENDOR technique and by using our measurements at other magnetic fields we are able to almost completely disentangle the spectrum.

The interaction between the Cr^{3+} ion and its Al nuclear neighbors has a strong effect on the behavior of the two-pulse electron-spin echo. Marked modulation of the echo amplitude as a function of the time separation between the excitation pulses has been observed.[9,13,14] Therefore, as an independent check of the validity of the Hamiltonian given in Eq. (12) and our determination of the parameters, we calculate the echo envelope modulation using Eq. (2.22) of Ref. 13 and compare the results with an experimental measurement of the modulation. We have obtained spin-echo data[14] at 9.31 and 16.24 GHz corresponding to the $-\frac{1}{2} \rightarrow +\frac{1}{2}$ transitions at 3.3 and 5.8 kG, and these experimental data are plotted as the middle curves of Fig. 11 and 12, respectively. The upper curves are calculated with the Hamiltonian and interaction parameters of Laurance *et al.*, while the lower curves are the theoretical spin-echo envelope calculated with the more general Hamiltonian and the parameters determined from our echo-ENDOR data. We include only the nearest 14 neighbors in our calculation. Note that all the interaction constants were determined by their respective ENDOR experiments and were not modified to improve the fit to the experimental echo envelope. The theoretical curves are therefore calculated with no adjustable parameters other than an exponential decay factor used to approximate dephasing terms not included in the Hamiltonian.

The agreement between experiment and theory

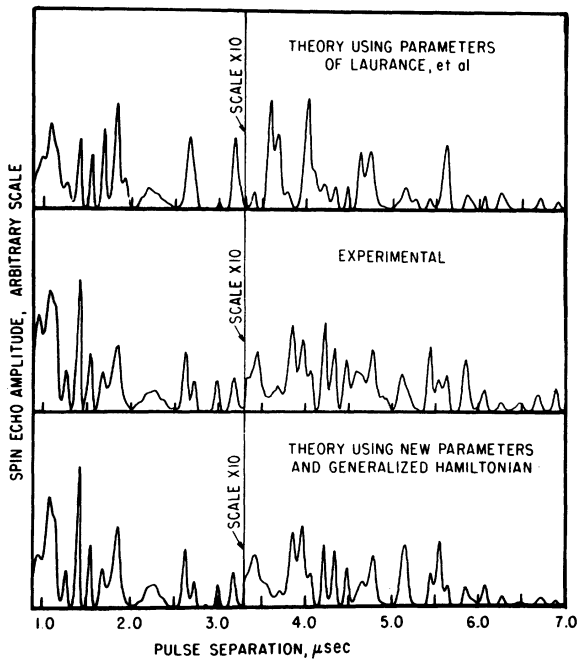

FIG. 11. Echo envelope modulation at 9.31 GHz, 3.3 kG.

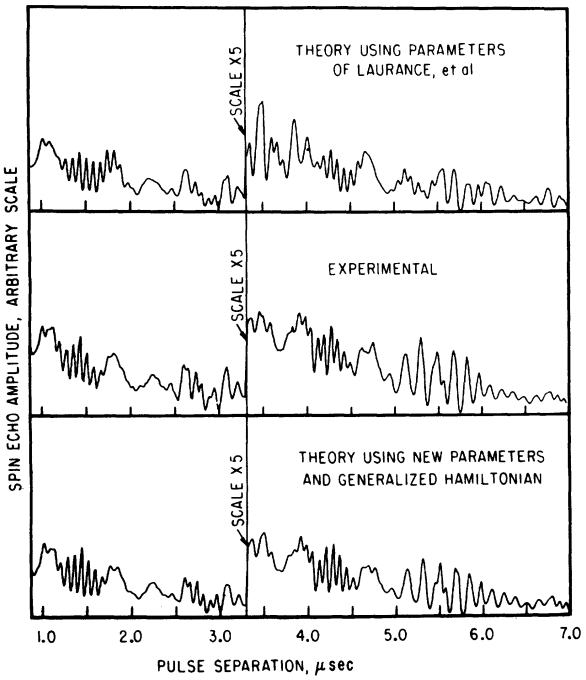

FIG. 12. Echo envelope modulation at 16.24 GHz, 5.8 kG.

is improved by using the lower theoretical curves. All of the 16.24-GHz data (Fig. 12) and the data of the 0.8- to 4.0-μsec region of the 9.31-GHz experiment (Fig. 11) agree very well with the theory. Furthermore, for pulse separations greater than 4.0 μsec at 9.31 GHz, the general features of the echo envelope behavior are found in the theoretical echo envelope. The echo modulation data provide an extremely sensitive check of our results. Note that except for the inclusion of the principal axis tilt, the asymmetry parameter, and the values of Q for the neighbor sets J and K, the redetermined parameters given in Table I are essentially unchanged from those of Laurance *et al.* In fact, at 5.8 kG the new constants produce only a maximum of about a 3% change in aluminum nuclear frequencies.

APPENDIX: SIMPLE VECTOR MODEL

Before any excitation pulses are applied, the electron-spin system is in equilibrium with the lattice, and, hence, there is a spin polarization along the direction of the dc magnetic field. We represent this polarization by the vector $\vec{P}_0$ in Fig. 13. For simplicity we analyze the motion of the spin magnetization in a frame of reference rotating about the direction of the applied dc magnetic field of the angular frequency Ω of the excitation pulses. Since these pulses are applied at exact resonance with the spin system, the spin polarization precesses about the magnetic field vector $\vec{H}_{rf}$ of the circularly polarized excitation pulse. This motion is indicated in Fig. 13(a) for the first excitation pulse where the polarization follows the dashed line until it has precessed 90° about $\vec{H}_{rf}$, at which time the excitation pulse is turned off. The individual spin moments which were aligned to form $\vec{P}_0$ begin to dephase because of their distribution in resonance frequencies. This dephasing is indicated in Fig. 13(b) for two groups of spins labeled 1 and 2, which have moved from the initial position by the angles θ_1 and $-\theta_2$ at the time the second 90° excitation pulse is applied. When this pulse is turned off, there is a further dephasing of the electron-spin moments such that a series of cones [Fig. 13(c)] is formed which preserves the phase information contained in the angles θ_1 and $-\theta_2$, etc., as the projection of the spin magnetization along the direction of the dc magnetic field. We have indicated this separately in Fig. 13(d) by the vectors with the labels e and g which are proportional to the probability that the associated spin is pointing down (spin in excited state) or pointing up (spin in ground state).

Let $\mathcal{P}(\theta)d\theta$ be that part of P_0 which has precessed into the region θ to $\theta+d\theta$ at the time the second 90° excitation pulse is applied. The as-

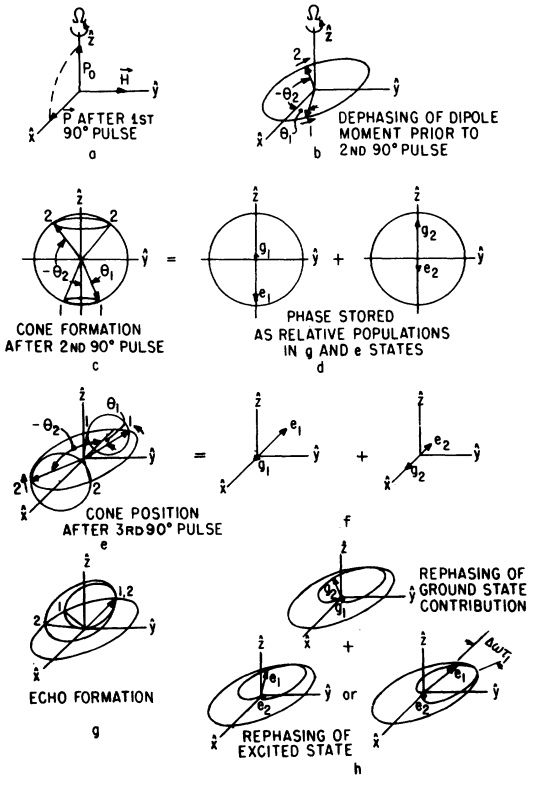

FIG. 13. Stimulated-echo formation with effect of double resonance (shown in bottom right-hand side of h).

sociated dipole density of "g" and "e" states after cone formation is obtained from the normalization and excess density conditions

$$\mathcal{P}(\theta)=\mathcal{P}_g(\theta)+\mathcal{P}_e(\theta)\,,\qquad \mathcal{P}(\theta)\cos\theta=\mathcal{P}_g(\theta)-\mathcal{P}_e(\theta)\,. \tag{A1}$$

We assume that the separation between the first and second 90° excitation pulses is long enough for complete dipole dephasing, which we express as $\mathcal{P}(\theta)=(1/2\pi)P_0$, so that

$$\mathcal{P}_g(\theta)=(1/4\pi)(1-\cos\theta)\,P_0\,,\qquad \mathcal{P}_e(\theta)=(1/4\pi)(1+\cos\theta)P_0\,, \tag{A2}$$

to give the length of the vectors in Fig. 13(d) with the labels g and e.

The application of a third 90° excitation pulse rotates the spin magnetization 90° as shown in Figs. 13(e) and 13(f). The conventional analysis of stimulated echo formation proceeds as in Fig. 13(g), where the individual magnetization cones are shown to all line up with a common edge at a time after the third excitation pulse equal to the time separation of the first two excitation pulses. Since all the magnetization cones have a common edge, there is a net nonzero magnetization and the echo is formed.

An alternative way of analyzing the problem which is superior for the treatment of our double-resonance experiment is to consider the echo as having arisen separately from spins which after cone formation are left either in the ground state or excited state, i.e., the vectors $\vec{\mathcal{P}}_g$ and $\vec{\mathcal{P}}_e$, respectively. At the time of the echo the ground-state vectors $\vec{\mathcal{P}}_g$ produce an ordered magnetization distribution given in polar form by

$$\mathcal{P}_g(\theta)=(1/4\pi)(1-\cos\theta)P_0\,, \tag{A3}$$

as shown in the upper diagram of Fig. 13(h). This equation is obtained from Eq. (A2), using the fact that at the time of the stimulated echo the ith dipole has precessed an angle θ_i from its position in Fig. 13(f). The same result is obtained for $\mathcal{P}_e$, so that the net moment is

$$\langle P\rangle=+2\int_0^{2\pi}d\theta\,(1/4\pi)(1-\cos\theta)\cos\theta P_0=-\tfrac{1}{2}P_0\,. \tag{A4}$$

The factor of $\frac{1}{2}$ reduction is caused by the dephasing in producing the cones.

In the case in which a double resonance is effected with the excited-state electron spins, the time development of $\mathcal{P}_g$ is unaffected; however, after the third excitation pulse the excited-state spins will rephase at a rate shifted by a fixed amount $\Delta\omega$ determined by $\hbar^{-1}$ times the interaction energy of the electron spins with the *resonated* nuclei. In polar form this becomes

$$\mathcal{P}_e(\theta)=(1/4\pi)[1-\cos(\theta+\Delta\omega\tau_1)]P_0\,. \tag{A5}$$

This distribution is shown in the lower-right-hand diagram of Fig. 13(h). Without double resonance $\Delta\omega\tau_1=0$ and the distribution to the left of this diagram obtains. The echo amplitude is determined by the vector sum of the ground- and excited-state dipole moments so that Fig. 13(h) shows the possible destructive or constructive interference effects which can be obtained.

*Work supported in part by the Joint Services Electronics Program under Contract No. DAABO7-69-C-0383.

[1]G. Makhov, C. Kikuchi, J. Lambe, and R. W. Terhune, Phys. Rev. **109**, 1399 (1958).
[2]T. H. Maiman, Nature (Lond.) **187**, 493 (1960).
[3]A. A. Manenkov and A. M. Prokhorov, Zh. Eksp. Teor. Fiz. **28**, 762 (1955) [Sov. Phys.-JETP **1**, 611 (1955)]; J. E. Geusic, Phys. Rev. **102**, 1252 (1956); E. O. Schultz-DuBois, Bell Syst. Tech. J. **38**, 271 (1959); A. A. Manenkov and A. M. Prokhorov, Zh. Eksp. Teor. Fiz. **38**, 1042 (1960) [Sov. Phys.-JETP **11**, 751 (1960)]; W. B. Mims and J. D. McGee, Phys. Rev. **119**, 1233 (1960); R. A. Armstrong and A. Szabo, Can. J. Phys. **38**, 1304 (1960); J. C. Gill, Proc. Phys. Soc. Lond. **79**, 58 (1962).
[4]S. Sugano and Y. Tanabe, J. Phys. Soc. Jap. **13**, 880 (1958); S. Sugano and I. Tsujikawa, J. Phys. Soc. Jap. **13**, 899 (1958).
[5]N. A. Kurnit, I. D. Abella, and S. R. Hartmann, Phys. Rev. Lett. **13**, 567 (1964).
[6]S. L. McCall and E. L. Hahn, Phys. Rev. Lett. **18**, 908 (1967).
[7]P. P. Crooker, G. A. Weeks, and E. C. Crittenden, Jr., Phys. Rev. **188**, 557 (1969).
[8]N. Laurance, E. C. McIrvine, and J. Lambe, J. Phys. Chem. Solids **23**, 515 (1962).
[9]D. Grischkowsky and S. R. Hartmann, Phys. Rev. Lett. **20**, 41 (1968).
[10]W. J. C. Grant and M. W. P. Strandberg, Phys. Rev. **135**, A727 (1964).
[11]R. F. Wenzel, Phys. Rev. B **1**, 3109 (1970).
[12]G. Feher, Phys. Rev. **103**, 834 (1956); Phys. Rev. **105**, 1122 (1957).
[13]D. Grischkowsky and S. R. Hartmann, Phys. Rev. B **2**, 60 (1970).
[14]P. F. Liao and S. R. Hartmann, Solid State Commun. **10**, 1089 (1972).
[15]P. F. Liao and S. R. Hartmann, Phys. Lett. A **38**, 295 (1972).
[16]W. B. Mims, Proc. R. Soc. Lond. **283**, 452 (1965).
[17]D. E. Kaplan and E. L. Hahn, J. Phys. Radium **19**, 821 (1958); M. Emshwiller, E. L. Hahn, and D. Kaplan, Phys. Rev. **118**, 414 (1960).
[18]E. L. Hahn, Phys. Rev. **80**, 580 (1950).
[19]J. P. Gordon, Rev. Sci. Instrum. **32**, 658 (1961).
[20]J. Lambe, N. Laurance, E. C. McIrvine, and R. W. Terhune, Phys. Rev. **122**, 1161 (1961).
[21]R. Fletcher and M. J. D. Powell, Comput. J. **6**, 163 (1963).
[22]A. H. Silver, T. Kushida, and J. Lambe, Phys. Rev. **125**, 1147 (1962).
[23]R. V. Pound, Phys. Rev. **79**, 685 (1950).